Communication

Nano-mechanical Behavior of H13 Tool Steel Fabricated by a Selective Laser Melting Method

VAN LUONG NGUYEN, EUN-AH KIM, JAECHEOL YUN, JUNGHO CHOE, DONG-YEOL YANG, HAK-SUNG LEE, CHANG-WOO LEE, and JI-HUN YU

Nano-mechanical properties of selective laser melted H13 steel at a scan laser speed of 100 mm/s were investigated using nanoindentation tests. The findings shed light on the interrelationship between the nanoindentation strain rate and hardness. It was found that the strain-rate sensitivity exponent ($m = 0.022$) of this material indicated that the nanoindentation hardness increased in a range of (8.41 to 9.18) GPa with an increase in the strain rate ranging from 0.002 to 0.1 s^{-1}.

https://doi.org/10.1007/s11661-018-5024-2

H13 is one of the most widely used hot work tool steels applied to casting molds, extrusion tool, and forging dies, *etc*. due to its strong temper resistance and ability to maintain high hardness and strength at elevated temperatures.[1–7] Hot work tool steels fabricated by conventional methods require expensive dedicated tools and thus are not suitable for small-scale production and the production of complex shapes.[5–7] An additive manufacturing (AM) technique, which builds parts from 3D digital models typically by a layer additive process, has been an effective method to solve these problems.[5–14] Accordingly, a selective laser melting (SLM) method, a laser powder-bed AM process, should be suitable for processing of H13 because it offers the ability to not only reduce the amount of machining and hence wastage of this expensive material but also to produce intricate molds with a nearly full density and a refined microstructure.[1–3,13]

The mechanical behavior of the H13 prepared by the SLM process is one of the most important characteristics and has been reported recently.[7,8,15–17] Micro-hardness (Vickers, Rockwell, and Briness) tests and tensile tests have been conducted to evaluate the mechanical behavior of the SLM-ed H13 tool steel.[7,8,15–17] To conduct those tests, many samples with large volumes had to be prepared and the mechanical behavior (hardness or tensile strength) was measured at only low loading rates (static) and in particular the creep behavior could not be evaluated. Meanwhile, nanoindentation tests could provide the strain-rate sensitivity of materials, especially for small-sized materials that are not suitable for the above test methods.[18–23] Nanoindentation tests should be therefore applied to study mechanical characteristics of SLM-ed H13 material.

However, many reports have noted that the correlation between the measured character from the indentation creep and those obtained from the conventional uniaxial tests are poor.[22,23] For example, Wang *et al.* reported that the creep rate under nanoindentation was typically excessive faster than that under uniaxial creep due to more complex and severe stress state under nanoindentation.[22] Shen *et al.* also claimed that the intrinsic discrepancy in the deformation mechanics caused the difference in the testing results by nanoindentation and uniaxial methods.[24] Specifically, the deformed volume of material is conserved throughout the process of creep deformation in conventional uniaxial creep tests, while the deformed area underneath the indenter in nanoindentation tests is continuously expanded to the adjacent area which did not deform previously. The newly deformed zone undergoes the primary creep process, which is different with creep rate of materials at or close the center of the deformed zone. The response from indentation creep tests thus includes transient stage as well as steady state, or even post steady-state stages, which is more complex than that from uniaxial tests.

Different methods have proven popular to measure the strain rate in the nanoindentation creep tests, *viz*., constant rate of loading (CRL), constant strain rate (CSR), constant load and hold (CLH), and strain rate jump (SRJ) tests.[21–28] Thereby, the CRL method is the technique in which a steady loading rate is used until the tip displacement rate becomes nearly constant; meanwhile, the CSR technique uses an exponential load–time function to produce a steady strain rate. Another method is the CLH test using a hold segment at steady load to achieve continually changing strain rate and hardness pairs, while the SRJ test uses various exponential loading rates to generate several strain rate and hardness pairs. In these methods, the CRL method

VAN LUONG NGUYEN, EUN-AH KIM, DONG-YEOL YANG, HAK-SUNG LEE, and JI-HUN YU are with the Powder & Ceramic Division, Korea Institute of Materials Science (KIMS), Changwon 51508, Korea and also with the Metal 3D Printing Convergence Research Team, Korea Institute of Machinery & Materials (KIMM), Daejeon 34103, Korea. Contact e-mail: jhyu01@kims.re.kr JAECHEOL YUN and JUNGHO CHOE are with the Powder & Ceramic Division, Korea Institute of Materials Science (KIMS). CHANG-WOO LEE is with the Metal 3D Printing Convergence Research Team, Korea Institute of Machinery & Materials (KIMM).

Manuscript submitted January 22, 2018
Article published online November 30, 2018

allows for a simple calculation of strain rates, and has produced good correlations to conventional values in tests on materials.[28] Therefore, the CRL method is chosen to measure the strain rate in this paper. To be specific, nanoindentation tests were conducted to probe the dependence of mechanical properties of H13 produced by SLM at 100 mm/s laser scan speed on the strain rate.

The powder material used in this study was commercially available H13 steel powder (Osprey Metals, Sandvik Osprey Ltd., Sweden) in a size range 10–45 μm. Its chemical composition is listed in Table I. The feedstock powders were processed by the SLM process (model name: a Concept LaserMlab-Cusing system) with parameters indicated in Table II. The H13 cuboid specimens ($10 \times 10 \times 10$ mm) are shown in Figure 1. The detailed preparation of the SLM process of this material can also be found in References 8, 11, 12. The cuboid specimens prepared by SLM were mounted in epoxy resin and then cross-sectioned to allow their microstructural observations.

To evaluate the mechanical properties of the SLM H13 steel, nanoindentation tests were performed for samples at room temperature on a NanoTest nanoindenter, supplied by Micro Materials Ltd., Wrexham, UK, using a three-sided Berkovich diamond indenter. The maximum load was chosen with sufficient magnitude to ensure that the indentation marks would be present in all phases of the samples. Specifically, all nanoindentation tests were carried out at the same maximum load (500 mN) and with loading rates of 50, 25, 16.67, 12.5, 10, 5, and 1 mN/s. The indenter was then held at the maximum load for 5 seconds, which was followed by unloading at a rate of 50 mN/s for all tests. At least ten indentation points at each loading rate were carried out and the results were averaged.

Figure 2 shows a typical load-depth curve used in nanoindentation. The hardness and Young's modulus were determined from the peak load and the initial slope of the unloading stage.[27] An indentation stress (σ), the representative stress from a nanoindentation test, is defined as the instantaneous load (P) divided by the projected contact area (A_c), which is also the definition of indentation hardness (H) measured in the course of loading process.[19,23] Moreover, during nanoindentation tests under a constant loading rate, indentation strain rate is a non-linear function of time that can be estimated from the depth–time data obtained for a given range of indentation depths.[28]

The indentation stress (σ) has an approximately linear relationship with the strain rate ($\dot{\varepsilon}$).[28] This relationship can be expressed by Eq. [1]:

$$\sigma = C\dot{\varepsilon}^m, \qquad [1]$$

where C is the material constant, and m is the strain-rate sensitivity exponent. Therefore, the strain-rate sensitivity exponent can be determined by the slope of a $\log\sigma$ *vs* $\log\dot{\varepsilon}$ plot.

Figure 3 presents a microstructure of SLM H13 in this work, thereby Figure 3(a) shows an optical microscope (OM) picture of the sample after etching in the magnification (50 times), while Figure 3(b) gives SEM micrograph of indentations on the surface of a SLM H13 specimen, and Figure 3(c) is a close-up view at the location of the indenter point indicated by the rectangle in Figure 3(b). In general, microstructure of a material prepared by the SLM process is significantly affected by

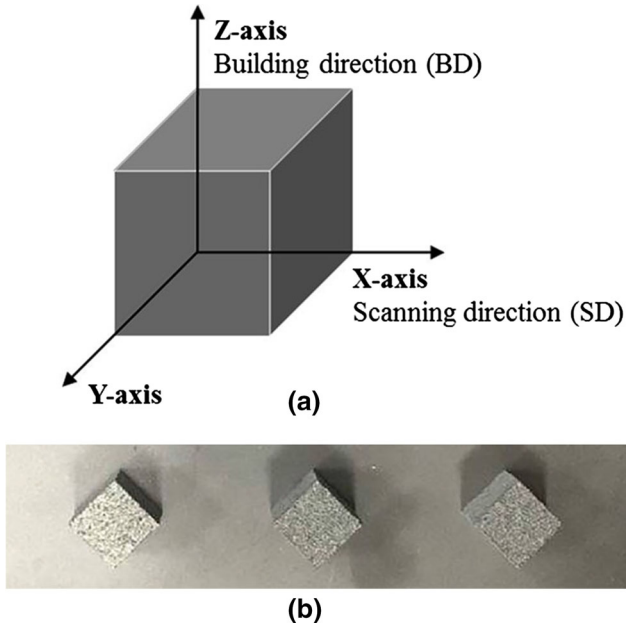

Fig. 1—(*a*) A cubic H13 specimen in this study and (*b*) samples produced by SLM.

Table I. Chemical Composition of H13 Powders for the SLM Process

Component	Fe	Cr	Mo	Mn	Si	V	C
Value (weight percent)							
Standard (Sandvik)	bal.	4.7 to 5.50	1.10 to 1.75	0.20 to 0.50	0.80 to 1.20	0.80 to 1.20	0.32 to 0.45
Analysis (ICP, C/S)	bal.	5.15	1.62	0.43	1.10	1.16	0.44

Table II. SLM Processing Parameters

Power	Scan Speed	Hatch Spacing	Layer Thickness	Atmosphere
90 W	100 mm/s	80 μm	25 μm	Argon

Table III. Chemical Composition (Atmospheric Percent) of Points A, B, and C of Fig. 3(b)

Point	C	Si	V	Cr	Mn	Fe	Mo
A	1.67	1.3	1.47	5.04	0.21	88.50	1.81
B	1.38	1.07	1.15	4.74	0.06	90.01	1.58
C	6.54	—	—	—	—	93.46	—

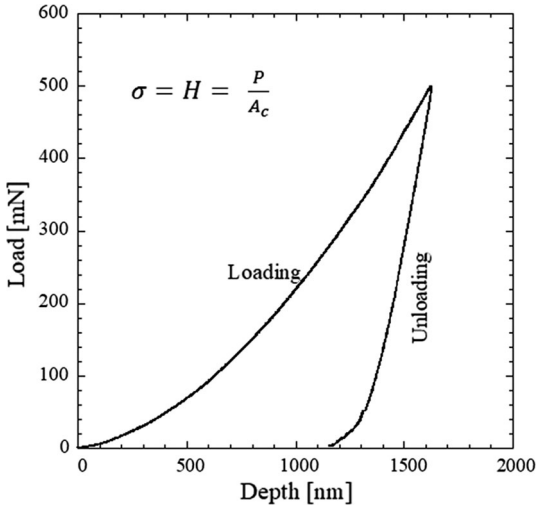

Fig. 2—An example of a typical load–depth curve.

the metallurgical bonding between the adjacent scan tracks and the neighboring layers.[12,15,29] A successful SLM process is a characterized by sufficiently high laser energy input, resulting a complete melting and subsequent sufficient solidification process, and hence, leading the positive bonding between adjacent scan tracks and the neighboring layers.[12,15,29] For the SLM H13 at the scan speed of 100 mm/s, excessive energy input induced by the much low scanning speed in this case, causing over-melting on the powder bed.[8] Thus, this results powder vaporization, spatter generation or gases trapped within the melt pool. As a result, spherical pores were formed during solidification process of SLM samples, and especially, the microstructure was composed of a granular phase surrounded by a cellular-shaped phase due to spatter generation, as shown at outside microstructure of the nanoindenter in Figure 3(c).

Using an image analysis program, the size of the granular phase was determined to be 1.42 μm, as shown in Figure 3(c). EDS results of points A (cellular-shaped phase), B (granular phase), and C indicated in Figure 3(c) are presented in Table III. The results show that the Fe content of point-A is greater than that of point-B, while the content of the remaining elements of point-A is less than that of the point-B. This indicated that the cellular-shaped phase is Fe-richer in content than the granular phase. On the other hand, from the results of the EDS analysis on chemical compositions at point-C, it is deduced that this phase formed in this work is Fe_3C carbide in the microstructure of the material together with the existence of cellular-shaped and granular phases.

Table IV. Results Obtained from Different Nanoindentation Strain Rates

Loading Rate (mN/s)	Strain Rate (s^{-1})	Hardness (MPa)
1	0.002	8.41
5	0.01	8.66
10	0.02	8.73
12.5	0.025	8.8
16.67	0.033	8.96
25	0.05	8.93
50	0.1	9.18

Figure 4 shows the typical displacement (depth–time) curves for the SLM specimens as obtained from nanoindentation tests under various loading rates. The strain rates were calculated from the data at a the steady stage in Figure 4 and the results were 0.1, 0.05, 0.033, 0.025, 0.02, 0.01, and 0.002 s^{-1}, corresponding to 50, 25, 16.67, 12.5, 10, 5, and 1 mN/s, respectively. As highlighted in Figure 4, the loading time to reach the same indentation depth increases significantly with the decreasing strain rate. Results from nanoindentation tests at different strain rates for the hardness, Young's modulus and the maximum depth of indentation are also presented in Table IV. It can be seen from Table IV that as the strain rate increases in the range of (0.002 to 0.1) s^{-1}, the hardness increases between 8.41 and 9.18 GPa.

Previously, Mencin *et al.* examined an H13 die steel specimen on room temperature using the nanoindentation method and reported that the hardness value of the material was 6.6 GPa.[6] In the present study, the hardness values of the SLM H13 samples at different strain rates were higher than that of the H13 prepared without the SLM process. This shows an improvement in mechanical properties due to effects of the SLM process. In this study, the hardness increases with the nanoindentation strain rate, showing that the brittleness of the H13 built by the SLM process will increase at higher strain rates.

In the previous research, the macro hardness of the SLM H13 samples at a laser scan speed of 100 mm/s was determined to be 51.04 HRC.[8] On the other hand, there was a relationship between nanoindenter hardness (GPa) and macro-hardness (HRC) for the H13 specimen.[6] Accordingly, the macro hardness value (51.04 HRC) corresponds to the nanoindenter hardness value (about 7.0 GPa), which is smaller than the values in this work. Because the hardness value increases with an increase of the strain rate, dynamic hardness values

measured from nanoindentation tests using relatively high strain rates are thus higher in this work as compared to the hardness value determined from conventional indentation tests at a very lower strain rate (static).

Figure 5 presents the relationship between indentation stress and strain rate with respect to the ($\log\sigma$–$\log\dot{\varepsilon}$) form. The equation in the figure indicates that the relationship between these two parameters has a high correlation coefficient (R = 0.97), implying that this function can properly measure the dependence of the nanoindentation stress on the strain rate. The slope of the straight line in Figure 5 represents the strain-rate sensitivity exponent (m), with a value of 0.022 for the SLM H13 sample at 100 mm/s.

The value of m has been used to evaluate the super-plasticity of materials, in which alloys with m values exceeding 0.3 often behave as superplastic materials.[3] The value of m (0.022) in this study does not exceed 0.1, which is similar to that of the most known materials. Moreover, no cracking was found on sample surfaces at all indenters, as shown in Figure 3(b), although the maximum level of the applied force of the nanoindentation machine was chosen under the change of the strain rate in this work. As a result, although the strain rate sensitivity is excessive lower than that of superplastic materials, the SLM H13 sample has the low crack sensitivity.

Some researchers have also measured the m parameter at room temperature to evaluate the mechanical

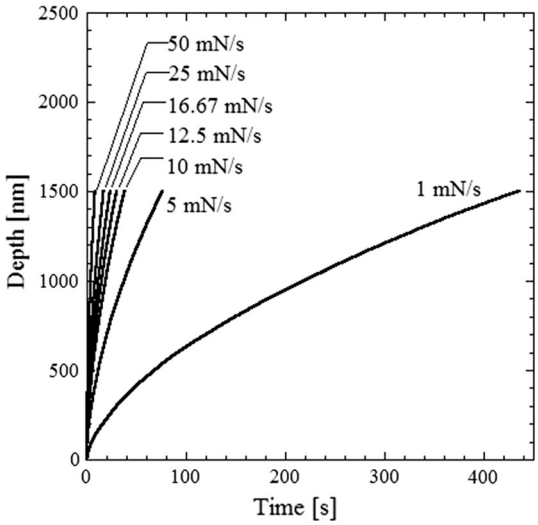

Fig. 4—Depth–time curves of H13 made by SLM at 100 mm/s of scan speed.

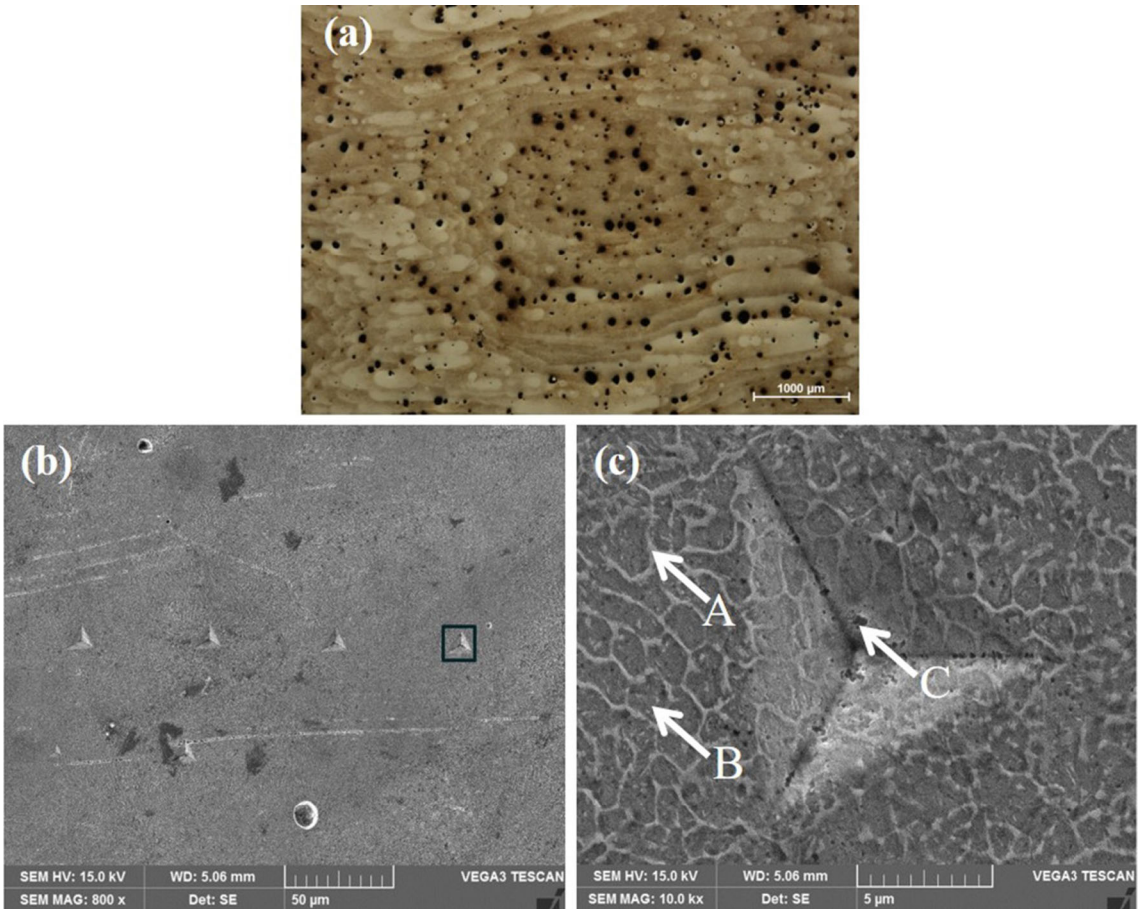

Fig. 3—(*a*) OM graph of a sample after etching in the magnification (50 times), (*b*) SEM micrograph of indentation points of H13 made by SLM at 100 mm/s of scan speed, and (*c*) close-up view at the location indicated by the rectangle in (b).

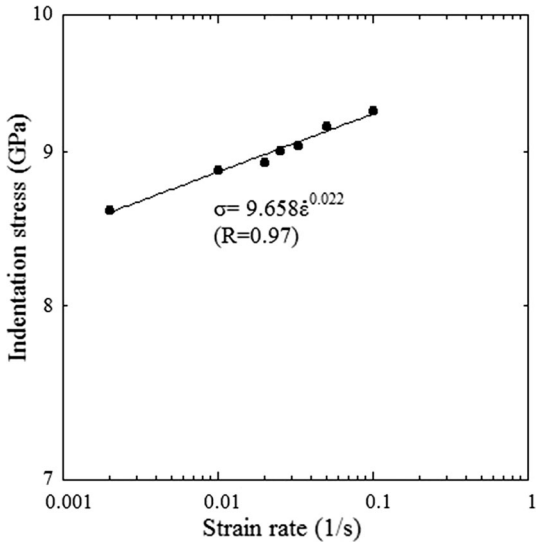

Fig. 5—Representative stress as a function of strain rate.

Table V. The Strain-Rate Sensitivity Value in This Study Along with Other Data for H13 Available in the Literature

Reference	Treatment	Test Method	Grain Size (μm)	m
3	annealing	tensile	30 to 40	0.31
3	quenching	tensile	4	0.26
This work	SLM	nanoindentation	1.4	0.022

properties of the H13 material.[3] Table V compares the strain-rate sensitivity exponent value of this study with data available in the literature. It is shown in Table V that the m value in this study is excessive smaller than others. Table V indicates that the H13 strain-rate sensitivity is directly proportional to the grain size. Our preliminary work on the effects of laser scan speed on the nano-mechanical behavior of the SLM H13 material also verifies this result, showing that m increases with the average grain size.[30] In addition, Table V indicates that the mechanical behavior of H13 made by SLM is less susceptible to the strain rate, as compared to that of heat-treated H13.

Overall, H13 steel prepared by SLM at 100 mm/s laser scan speed was studied. In addition to the existence of Fe_3C carbide, the material microstructure revealed a granular phase with a size of 1.42 μm surrounded by a cellular-shaped Fe-richer phase. Using a nanoindentation technique, the hardness (representative stress) of the SLM H13 material was found to be susceptible to the strain rate with a strain-rate sensitivity exponent (m) of 0.022. Specifically, the hardness increased from 8.41 to 9.18 GPa as the nanoindentation strain rate increased in the range of 0.002 and 0.1 s^{-1}. Furthermore, there were no cracks on the sample surfaces at indenter points, reflecting the low crack sensitivity of the SLM H13 steel. Through a comparison to results from other studies, it is deduced that the nanoindentation strain-rate sensitivity of the H13 steel is directly proportional to the grain size.

This study was supported by the Fundamental Research Program of the Korea Institute of Materials Science (Development of High Performance Materials and Processes for Metal 3D Printing).

OPEN ACCESS

REFERENCES

1. J. Pinkerton and L. Li: *Int. J. Adv. Manuf. Technol.*, 2005, vol. 25, pp. 471–79.
2. J. Marashi, E. Yakushina, P. Xirouchakis, R. Zante, and J. Foster: *J. Mater. Process. Technol.*, 2017, vol. 246, pp. 276–84.
3. Z. Duan, W. Pei, X. Gong, and H. Chen: *Materials*, 2017, vol. 10, pp. 870–78.
4. M. Kang, G. Park, J.G. Jung, B.H. Kim, and Y.K. Lee: *J. Alloy. Compd.*, 2015, vol. 627, pp. 359–66.
5. J.J. Yan, D.L. Zheng, H.X. Li, X. Jia, J.F. Sun, and Y.L. Li: *Metals*, 2017, vol. 52, pp. 12476–85.
6. P. Mencin, C.J.V. Van Tyne, and B.S. Levy: *J. Mater. Eng. Perform.*, 2009, vol. 18, pp. 1067–72.
7. J. Safka, M. Ackermann, and L. Volesky: *J. Phys. Conf. Ser.*, 2016, vol. 709 (012004), pp. 1–7.
8. J.C. Yun, J.H. Choe, H.N. Lee, K.B. Kim, S.S. Yang, D.Y. Yang, Y.J. Kim, C.W. Lee, and J.H. Yu: *J. Korean. Powder. Metall. Inst.*, 2017, vol. 24 (3), pp. 195–201.
9. N.T. Aboulkhair, C. Tuck, I. Ashcroft, I. Maskery, and N.M. Everitt: *Metall. Mater. Trans. A*, 2015, vol. 46A, pp. 3337–41.
10. V.S. Sufiiarov, A.A. Popovich, E.V. Borisov, I.A. Polozov, D.V. Masaylo, and A.V. Orlov: *Proc. Eng.*, 2017, vol. 174, pp. 126–34.
11. J.P. Choi, G.H. Shin, M. Brochu, Y.J. Kim, S.S. Yang, K.T. Kim, D.Y. Yang, C.W. Lee, and J.H. Yu: *Mater. Trans.*, 2016, vol. 57, pp. 1952–59.
12. J.P. Choi, G.H. Shin, S.S. Yang, D.Y. Yang, J.S. Lee, M. Brochu, and J.H. Yu: *Powder. Technol.*, 2017, vol. 310, pp. 60–66.
13. B. AlMangour, D. Grzesiak, and J.M. Yang: *J. Mater. Process. Technol.*, 2017, vol. 244, pp. 344–53.
14. J.P. Choi, G.H. Shin, H.S. Lee, D.Y. Yang, S.S. Yang, C.W. Lee, M. Brochu, and J.H. Yu: *Mater. Trans.*, 2017, vol. 58, pp. 294–97.
15. J. Sander, J. Hufenbach, L. Giebeler, H. Wendrock, U. Kuhn, and J. Eckert: *Mater. Des.*, 2016, vol. 89, pp. 335–41.
16. R. Mertens, B. Vrancken, N. Holmstock, Y. Kinds, J.P. Kruth, and J.V. Humbeeck: *Phys. Proc.*, 2016, vol. 83, pp. 882–90.
17. M.J. Holzweissig, A. Taube, F. Brenne, M. Schaper, and T. Niendorf: *Metall. Mater. Trans. B*, 2015, vol. 46B, pp. 545–49.
18. J.J. Hu, Y.S. Zhang, W.M. Sun, and T.H. Zhang: *Crystals*, 2018, vol. 8, p. 9.

19. S. Xu, A.H. Habib, A.D. Pickel, and M.E. McHenry: *Prog. Mater. Sci.*, 2015, vol. 67, pp. 95–160.
20. V.L. Nguyen, C.S. Chung, and H.K. Kim: *Mater. Lett.*, 2016, vol. 162, pp. 185–90.
21. C.Z. Liu and J. Chen: *Mater. Sci. Eng. A*, 2007, vol. 448, pp. 340–44.
22. C.L. Wang, Y.H. Lai, J.C. Huang, and T.G. Nieh: *Scripta Mater.*, 2010, vol. 62, pp. 175–78.
23. R. Goodall and T.W. Clyne: *Acta. Mater.*, 2006, vol. 54, pp. 5489–99.
24. L. Shen, W.C.D. Cheong, Y.L. Foo, and Z. Chen: *Mater. Sci. Eng. A*, 2012, vol. 532, pp. 505–10.
25. V.M. Kiener and K. Durst: *JOM*, 2017, vol. 69, pp. 2246–54.
26. P.S. Phani, W.C. Oliver, and G.M. Pharr: *JOM*, 2004, vol. 69, pp. 2229–36.
27. W.C. Oliver and G.M. Pharr: *J. Mater. Res.*, 2004, vol. 19, pp. 3–20.
28. M.J. Mayo and W.D. Nix: *Acta. Metall.*, 1988, vol. 36, pp. 2183–92.
29. Y.L. Li and D.D. Gu: *Mater. Des.*, 2014, vol. 63, pp. 856–67.
30. V.L. Nguyen, E.A. Kim, J.C. Yun, J.H. Choe, D.Y. Yang, H.S. Lee, C.W. Lee, J.H. Yu, (unpublished work).